Table VII. Localized MO's for S_4N_4 and S_2N_2: Minimal spd Results

S_4N_4

		S			N	
	% localizn	3s	3p	3d	2s	2p
S–N (×8)	97.98	26.6	69.9	3.5	12.9	87.2
S–S (×2)	92.03	15.1	83.9	1.0	0	0
LP_S (×4)	97.64	54.6	45.3	0.1	0	0
LP_N (×8)	84.0	0	0	0	41.1	58.9

S_2N_2

		S			N	
	% localizn	3s	3p	3d	2s	2p
S–N (×4)	97.8	21.3	74.8	3.9	26.0	74.0
S–N (×2)	96.5	11.7	85.2	3.1	15.4	84.6
$LP_S(\sigma)_A$	98.5	64.5	35.5	0	0	0
$LP_S(\sigma)_B$	98.3	62.5	37.5	0	0	0
$LP_S(\pi)_A$	92.9	0	99.6	0.4	0	0

axis but (in our hands) by only 0.06 Å, corresponding to an angle SCS of 2.6°.

Overall, therefore, and in agreement with the findings of ref 16, 17, and 19, we conclude that the molecule best fits the Lewis structure (**8**). The population analyses also show the

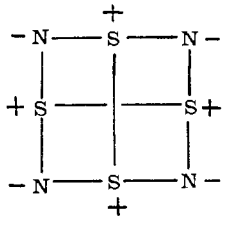

8

tendency towards S^+–N^- character required by the classical structure (**8**).

The valence-shell LMO's of S_2N_2 show a number of characteristics in common with the features deduced from semiempirical studies,[11] although in the present work σ and π MP's were allowed to mix, thus leading to "bent" bonds rather than pure σ or π LMO's.[11] The final LMO wave function corresponds to the structure (**9**), i.e., a single canonical form based on the pair resonance hybrids that can be drawn for a combination of S^{II} and S^{IV} bonding. The initial canonical

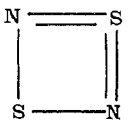

9

wave function is of course symmetrical, and the present form clearly shows the equivalence of the two S^{II} and S^{IV} centers. A consequence of this is that the two σ LP_S are not strictly identical since a σ/π separation has occurred at one side of the molecule and not at the other. The low level of delocalization of π LP_S is reminiscent of the CNDO-2 wave function.[11,12] The absence of cross-ring bonding, as noted above from the negative overlap populations, is also confirmed.

Concluding Remarks

The earlier work on the photoelectron spectra of S_2N_2 and S_4N_4 has been extended by the measurement of the He II spectra. Detailed interpretation of the data for S_4N_4 is difficult, but the new He II measurements, in conjunction with XPS data and the ab initio calculations by using more than one basis set, lead to a plausible interpretation for the complete valence-shell spectrum. This assignment differs significantly from that advanced on the basis of earlier semiempirical calculations. In contrast, the spectrum of S_2N_2 is relatively straightforward in assignment. The present results are in substantial agreement with those of earlier work, except that the first IP is assigned to a π_S rather than a π_N level.

A general feature emerging from the calculations, and consistent with the experimental photoelectron spectra, is that interactions among "lone-pair" orbitals are important in the sulfur nitrides. In the case of S_2N_2 these lead to a very large "through-space" splitting of $LP_S^{\pm}$ and $LP_N^{\pm}$ levels. The situation in S_4N_4 is more complicated, but the unexpected occurrence of the totally symmetric LP_N level as one of the most weakly bound orbitals is best interpreted in terms of through-space interactions between symmetric LP_S and LP_N group orbitals.

The conversion of our wave functions to a localized basis shows the absence of cross-ring N–N bonding and the presence of significant S–S bonding between each of the pairs of adjacent sulfur atoms in S_4N_4. By contrast, there is no cross-ring bonding in S_2N_2.

Registry No. **1**, 28950-34-7; **2**, 25474-92-4; SN, 12033-56-6; SN^+, 27954-72-9.

Contribution from the Inorganic Chemistry Laboratory, Oxford, OX1 3QR, Great Britain, and the Department of Chemistry, University of Edinburgh, Edinburgh, EH9 3JJ, Great Britain

Electronic Structure of the Group 5 Oxides: Photoelectron Spectra and ab Initio Molecular Orbital Calculations

RUSSELL G. EGDELL,* M. H. PALMER, and R. H. FINDLAY

Received July 30, 1979

Gas phase He I and He II photoelectron spectra of the group 5 oxides P_4O_6, As_4O_6, Sb_4O_6, and P_4O_{10} are reported. Qualitative descriptions of the electronic structure of these molecules are discussed with reference to ab initio molecular orbital calculations for the species P_4, P_4O_6, and P_4O_{10}. On the basis of the experimental and theoretical results, correlations among electronic energy levels within the series (i) P_4, P_4O_6, and P_4O_{10} and (ii) P_4O_6, As_4O_6, and Sb_4O_6 are suggested.

Introduction

The group 5 oxides are introduced in many chemistry textbooks as prototype examples of cage inorganic structures.[1] Recent interest in cage and cluster compounds has been stimulated by the belief that they may serve as molecular "models" for solid-state systems.[2]

* To whom correspondence should be addressed at the Inorganic Chemistry Laboratory, Oxford.

(1) E.g.: Huheey, J. E. "Inorganic Chemistry"; Harper and Row: London, 1975.
(2) E.g.: Muetterties, E. L. *Science* **1977**, *196*, 4292.

0020-1669/80/1319-1314$01.00/0

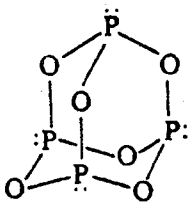

Figure 1. The valence-bond structure of P_4O_6.

Table I. Ionization Energy Data for P_4O_6, As_4O_6, and Sb_4O_6

IE, eV			
P_4O_6	As_4O_6	Sb_4O_6	assignt
10.55	10.05	9.31	
	10.32	9.55	$5t_2$ (M lone pair)
	10.55	9.82	
12.79	11.49	10.55	$3a_1$ (M lone pair)
			2e (M-O bonding)
			$2t_1$ (O lone pair)
13.90	12.46	11.37	$4t_2$ (O lone pair)
15.84	13.93	12.68	$3t_2$ (M-O bonding)
17.98	15.63	13.86	$1t_1$ (M-O bonding)
			$2a_1$ (M *ns*)
21.71 (II)[a]	20.37 (II)[a]	17.72 (II)[a]	$2t_2$ (M *ns*)

[a] (II) indicates that calibration is taken from the He II spectrum. The numbering scheme for MO's ignores those correlating with core levels of the M or O atom. Classification of orbitals under our qualitative scheme is given in parentheses.

From the formal point of view the oxides M_4O_6 may be derived from the parent-metal tetrahedra (M_4) by interlacing an octahedron of oxygen atoms. However, the M–M distances in the oxides are much larger than in the elemental tetrahedra.[3,4] It is usually assumed that the bonding is best represented in terms of classical valence-bond structures such as that depicted in Figure 1, cross-cage interactions being neglected.

The molecule P_4O_6 resembles the phosphite esters and PF_3 in that it forms complexes with acceptor species. Well-characterized examples include $P_4O_6(Ni(CO)_3)_4$[5,6] and $P_4O_6(BH_3)_2$.[7,8] It follows then that the relationship between P_4O_6 and P_4O_{10} is analogous to that between PF_3 and POF_3. In both cases the phosphorus(V) species may be regarded as a donor–acceptor complex between an oxygen atom and the corresponding phosphorus(III) species.

The oxides P_4O_6, P_4O_{10} and As_4O_6 have been studied from the stereochemical point of view by techniques such as electron diffraction[3,4] and Raman spectroscopy.[9,10] It appears that like the elemental M_4 species (M = P, As, Sb) the oxide molecules M_4O_6 (M = P, As, Sb) and P_4O_{10} posses full tetrahedral symmetry. Tetrahedral cage units also persist in the cubic arsenolite phase of As_4O_6 and the cubic senarmontite phase of Sb_4O_6.[11]

Despite the widespread interest in the stereochemical properties of the group 5 oxides, little attention has been devoted to their electronic structure. In the present communication we report He I and He II photoelectron (PE) spectra of the oxides M_4O_6 (M = P, As, Sb) and P_4O_{10}. The spectra are assigned by reference to ab initio MO calculations for the phosphorus species P_4, P_4O_6, and P_4O_{10}. The electronic structure of P_4, by contrast, has been the object of several experimental[12–14] and theoretical[12,15–18] investigations. A particular aim of the present work then was to explore the

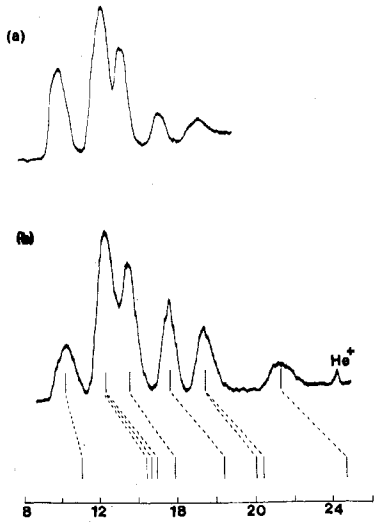

Figure 2. (a) He I and (b) He II PE spectra of P_4O_6. Note correlation between experimental ionization energies and those deduced by application of Koopmans' theorem to ab initio orbital energies (horizontal axis: ionization energy/eV).

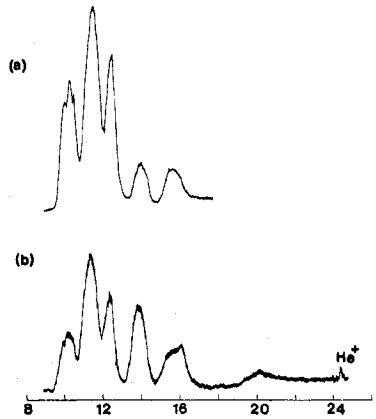

Figure 3. (a) He I and (b) He II PE spectra of As_4O_6 (horizontal axis: ionization energy/eV).

Table II. Ionization Energy Data for P_4O_{10}

IE, eV	assignt	IE, eV	assignt
13.40	$3t_1$ (apical O pπ)	16.54	$5t_2$ (O lone pair)
13.92	$7t_2$ (apical O pπ)	18.37 (II)[b]	$4t_2$ (P-O bonding)
14.44 (sh)[a]	3e (apical O pπ)	20.80 (II)[b]	$1t_1$ (P-O bonding)
14.76 (sh)[a]	$6t_2$ (P lone pair)		$3a_1$ (P 3s)
15.36	$6t_2$ (O lone pair)	23.83 (II)[b]	$3t_2$ (P 3s)
	2e (P-O bonding)		
	$4a_1$ (P lone pair)		

[a] (sh) indicates a shoulder. [b] (II) indicates that calibration is taken from He II spectra. The classification for the MO's is based on correlation with corresponding levels in P_4 and P_4O_6 and does not necessarily indicate dominant atomic populations (see text).

(3) Maxwell, L. R.; Hendricks, S. B.; Deming, L. S. *J. Chem. Phys.* **1937**, *5*, 626.
(4) Hampson, G. C.; Stosick, A. J. *J. Am. Chem. Soc.* **1938**, *60*, 1814.
(5) Riess, J. G.; Van Wazer, J. R. *J. Am. Chem. Soc.* **1966**, *88*, 2166.
(6) Riess, J. G.; Van Wazer, J. R. *J. Am. Chem. Soc.* **1965**, *87*, 5506.
(7) Riess, J. G.; Van Wazer, J. R. *J. Am. Chem. Soc.* **1966**, *88*, 2339.
(8) Kodama, G.; Kondo, H. *J. Am. Chem. Soc.* **1966**, *88*, 2045.
(9) Chapman, A. C. *Spectrochim. Acta, Part A* **1968**, *24*, 1687.
(10) Beattie, I. R.; Livingston, K. M. S.; Ozin, G. A.; Reynolds, D. J. *J. Chem. Soc. A* **1970**, 449.
(11) Almin, K. E.; Westgren, A. *Ark. Kemi, Mineral. Geol.* **1942**, *15*, 22.
(12) Brundle, C. R.; Kuebler, N. A.; Robin, M. B.; Basch, H. *Inorg. Chem.* **1972**, *11*, 20.
(13) Evans, S.; Joachim, P. J.; Orchard, A. F.; Turner, D. W. *Int. J. Mass Spectrom. Ion Phys.* **1972**, *9*, 41.
(14) Banna, M. S.; Frost, D. C.; McDowell, C. A.; Wallbank, B. *J. Chem. Phys.* **1977**, *66*, 3509.
(15) Hillier, I. H.; Saunders, V. R. *Chem. Commun.* **1970**, 1223.
(16) Dupvis, M.; King, M. F. *Int. J. Quantum Chem.* **1977**, *11*, 613.
(17) Archibald, R. M.; Perkins, P. G. *Chem. Commun.* **1970**, 569.
(18) Issleit, K.; Grundler, W. *Theor. Chim. Acta* **1968**, *11*, 107.

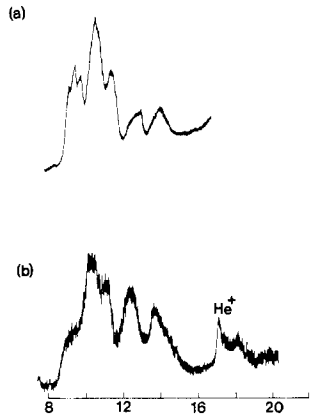

Figure 4. (a) He I and (b) He II PE spectra of As_4O_6 (horizontal axis: ionization energy/eV).

relationship between the electronic structure of phosphorus (P_4) and its oxides.

Experimental Section

A sample of P_4O_6 which had previously been used as a ^{31}P NMR standard was kindly provided by Dr. R. K. Mackie (Dundee University). The NMR tube was cracked in vacuo in a specially constructed vessel attached to the volatile inlet system of the PE spectrometer.

Commercial samples of As_4O_6, Sb_4O_6, and P_4O_{10} were used in spectroscopic investigations, following purification by sublimation in vacuo. The purified samples were handled in a dry atmosphere.

PE spectra were measured on a Perkin-Elmer PS 16/18 spectrometer modified by the inclusion of a hollow-cathode discharge lamp, high-current power supply, and multiscaler data acquisition system. Spectra were obtained at the following temperatures: P_4O_6, 25 °C; As_4O_6, 160 °C; Sb_4O_6, 410 °C; P_4O_{10}, 170 °C.

Spectra were calibrated by reference to peaks due to admixed methyl iodide, nitrogen, and noble gases, helium self-ionization peaks serving as additional calibration lines in He II spectra. There was no indication of reaction between calibrant gases and the sample under investigation. The half-width of the He I excited Ar 3p or $N_2(\tilde{X}^2\Sigma_g)$ line was typically around 50 meV under operating conditions.

PE spectra are shown in Figures 2–5 while ionization energy data are collected in Tables I and II. The reported ionization energies should be accurate to ±0.05 eV.

Computational Details

It was considered desirable to use the same basis set for calculations on each of the molecules P_4, P_4O_6, and P_4O_{10}. Thus the size of the basis set was restricted by limitations upon the number of electron repulsion integrals which could be accommodated in the calculation on P_4O_{10}. We used Gaussian basis sets[19] 10s 6p(×3) 1d(×6) and 7s 3p(×3) for phosphorus and oxygen, respectively. The six 3d functions on each P atom were contracted to the chemical 3d(×5) set plus an additional s orbital (3s′). The 10s 6p(×3) set was contracted to a minimal basis, so that the final set of phosphorus orbitals was 1s 2s 3s 3s′ 2p(×3) 3p(×3) 3d(×5) while that for oxygen was 1s 2s 2p(×3). These yielded a total energy of 1360.71 au for the P_4 molecule. This is marginally poorer than the total energy obtained by Brundle et al. (−1362.00 au),[12] who employed an 11s 7p basis for phosphorus, but represents a distinct improvement on the total energy (−1348.08 au) obtained by Hillier and Saunders.[15] The orbital sequence obtained in our calculation is identical with that of Brundle et al. However, it emerges from our calculation that the P_4 molecule is stable with respect to decomposition into four phosphorus atoms (binding energy = 0.46 au, ~12 eV), a result in accord with thermodynamic expectations but not predicted by the earlier calculation.[12] Omission of the phosphorus 3d function from the basis set leads to a total energy for P_4 greater than that for four phosphorus atoms.

Discussion

Electronic Structure of the Group 5 Oxides. A qualitative description of the electronic structure of the cage molecules M_4O_6 is easily developed by using a set of local bond and

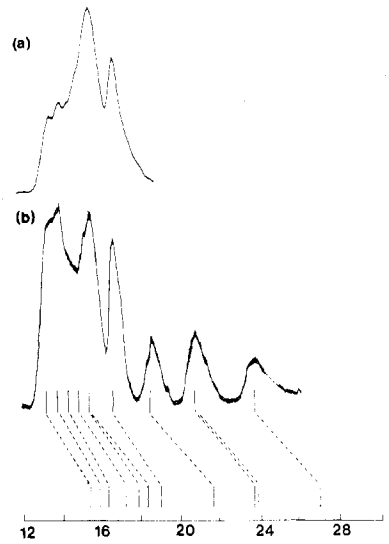

Figure 5. (a) He I and (b) He II PE spectra of P_4O_{10}. Note correlation between experimental ionization energies and those deduced by application of Koopmans' theorem to ab initio orbital energies (horizontal axis: ionization energy/eV).

stereochemical (sp^3) lone-pair functions as the basis for construction of molecular orbitals. Moreover, it is useful to consider local combinations of bonds and lone pairs which are either (i) symmetric or (ii) antisymmetric at the oxygen centers. With this approach we find that the local functions span irreducible representations of the tetrahedral point group as follows: M lone pair, $t_2 + a_1$; O lone pair (symmetric), $a_1 + t_2 + e$; O lone pair (antisymmetric), $t_1 + t_2$; M–O bonds (symmetric), $a_1 + t_2 + e$; M–O bonds (antisymmetric), $t_1 + t_2$.

Of course there will be significant interactions among combinations within a given symmetry manifold. Consideration of these interactions leads one toward a qualitative classification scheme for the molecular orbitals based on their dominant localization tendencies. One can be guided here by a number of simple ideas, for example, that combinations of orbitals which are in-phase at atomic centers should possess substantial atomic character. This leads to a classification of the molecular orbitals as follows: M lone pairs, $a_1 + t_2$; O lone pairs, $t_1 + t_2$; M–O bond orbitals, $t_1 + t_2 + e$; M *n*s orbitals, $a_1 + t_2$; O 2s orbitals, $t_2 + a_1 + e$. In this new scheme the M lone pairs correspond roughly to sp^n hybrid stereochemical lone pairs, whereas the O lone pairs are essentially O 2p orbitals orthogonal to the local M–O–M planes. Population analyses on the molecular orbitals derived from the ab initio calculations support the general features of our qualitative classification scheme, although in just a few cases interactions within a given symmetry manifold lead to molecular orbitals having atomic compositions different to those expected on simple grounds. In particular we note that the $2a_1$ MO of P_4O_6, which correlates with the P 3s dominated $1a_1$ MO of P_4, possesses surprisingly little P 3s atomic character.

Some guidance as to the relationship between electronic structures of P_4O_6 and P_4O_{10} is provided by treating the apical oxygen atoms as acceptor species which can receive electron density from the phosphorus lone-pair orbitals. This effect is clearly expected to stabilize the a_1 and t_2 lone-pair combinations. In addition the oxygen 2 p orbitals orthogonal to the local P–O axes give rise to symmetry orbitals spanning the new irreducible representation $t_1 + t_2 + e$. Of course a further influence of the apical oxygen atoms may be to perturb the pattern of interactions between orbitals within a particular symmetry manifold, leading to differences in atomic composition of molecular orbitals formally correlating with one an-

(19) Roos, B.; Siegbahn, P. *Theor. Chim. Acta* **1970**, *17*, 209.

Table III. Orbital Energies for P_4[a]

	orbital energy, eV			orbital energy, eV	
orbital[b]	sp	spd + 3s′	orbital[b]	sp	spd + 3s′
$1a_1$	−31.69	−28.78	$2t_2$	−11.36	−10.90
$1t_2$	−19.25	−19.28	1e	−10.84	−10.05
$2a_1$	−12.61	−12.80			

[a] E_{total}: sp, −1360.161 63 au; spd + 3s′, −1360.707 69 au. [b] The numbering scheme for the MO's ignores those correlating with core levels of the O or P atoms.

Table IV. Orbital Energies for P_4O_6[a]

	orbital energy, eV			orbital energy, eV	
orbital[b]	sp	spd + 3s′	orbital[b]	sp	spd + 3s′
$1a_1$	−41.06	−40.54	$3t_2$	−17.85	−18.44
$1t_2$	−38.26	−38.21	$4t_2$	−15.72	−15.93
1e	−36.41	−36.80	2e	−14.73	−14.99
$2t_2$	−24.86	−24.74	$2t_1$	−14.52	−14.70
$2a_1$	−20.14	−20.48	$3a_1$	−14.34	−14.44
$1t_1$	−19.37	−20.06	$5t_2$	−10.80	−11.06

[a] E_{total}: sp, −1808.132 59 au; spd + 3s′, −1808.909 91 au. [b] The numbering scheme for the MO's ignores those correlating with core levels of the O or P atoms.

other in the two molecules P_4O_6 and P_4O_{10}. Clarification on this point is provided by Mulliken population analyses of the wave functions derived from our ab initio MO calculation. We find that changes in molecular orbital composition in going from P_4O_6 to P_4O_{10} are generally rather small. However it is surprising to find that the levels $5t_2$ and $3a_1$, which correlate with phosphorus lone-pair levels of P_4O_6, have very little phosphorus character in P_4O_{10}. The three leading molecular subshells in P_4O_{10} are of t_1, t_2, and e symmetries and are predominantly of apical oxygen $2p_\pi$ character. However, each has a significant contribution from phosphorus 3d orbitals. This suggests that an important element in the apical O–P bonding is provided by π back-donation into the empty phosphorus 3d subshell.

Ideas about the bonding in P_4O_{10} may be further developed by considering a localized orbital description of the electron distribution. Conversion of the total wave function to a set of localized orbitals using the Foster–Boys method[20,21] gave a high degree of localization, with >96.5% of the electron density in two-center bonds or one-center lone pairs. In view of these observations it is apparent that cross-cage interactions in the form of cross-cage bonds must be small, although there is clearly cross-cage interaction in the sense that P and O levels belonging to different irreducible representations are nondegenerate.

Although the expected ether oxygen linkages (–O–) were obtained, at first sight the degree of covalency at phosphorus was six (>P≡O:). A similar phenomenon has been noted for the molecules X_3PO (X = F, Cl)[22] and is inevitable given the presence of a C_3 symmetry axis. More detailed examination of the localized wave function for P_4O_{10} showed the apical oxygen lone pair to be an $sp^{0.5}$ hybrid pointing away from the phosphorus atom. The three equivalent phosphoryl–oxygen bonds are in reality localized largely on the oxygen atom (78% and 74% in sp and spd basis, respectively) and are of high oxygen 2p character. The 22% (sp) or 24% (spd) phosphorus character is distributed 1:4 between s and p orbitals in the s:p basis and 1:3.7:1.2 between s, p, and d orbitals in the s:p:d

(20) Foster, J. M.; Boys, S. F. *Rev. Mod. Phys.* **1960**, *32*, 300.
(21) Boys, S. F. In "Quantum Theory of Atoms, Molecules and the Solid State"; Lowdin, P. O., Ed.; Academic Press: New York, 1966.
(22) Guest, M. F.; Hillier, I. H.; Saunder, V. R. *J. Chem. Soc., Faraday Trans. 2* **1972**, *68*, 867.

Table V. Orbital Energies for P_4O_{10}[a]

	orbital energy, eV			orbital energy, eV	
orbital[b]	sp	spd + 3s′	orbital[b]	sp	spd + 3s′
$1a_1$	−45.61	−44.68	$5t_2$	−18.30	−19.04
$1t_2$	−42.60	−42.20	$2t_1$	−17.49	−18.29
1e	−40.24	−40.44	2e	−17.34	−18.23
$2t_2$	−38.86	−39.14	$4a_1$	−17.09	−17.88
$2a_1$	−38.65	−38.97	$6t_2$	−15.78	−17.21
$3t_2$	−27.73	−27.22	3e	−15.62	−16.34
$1t_1$	−23.89	−23.96	$7t_2$	−14.55	−15.99
$3a_1$	−23.20	−23.80	$3t_1$	−13.88	−15.45
$4t_2$	−21.17	−21.71			

[a] E_{total}: sp, −2105.962 87 au; spd + 3s′, −2107.428 78 au. [b] The numbering scheme for the MO's ignores those correlating with core levels of the O or P atoms.

Table VI. Atomic Populations in Molecular Orbitals of P_4

	atomic pop., %				atomic pop., %		
orbital	3s	3p	3d	orbital	3s	3p	3d
$1a_1$	58	25	16	$2t_2$	11	83	5
$1t_2$	54	26	19	1e	0	99	1
$2a_1$	23	67	10				

Table VII. Atomic Populations in Molecular Orbitals of P_4O_6

	atomic pop., %				
	P			–O–	
orbital	3s	3p	3d	2s	2p
$1a_1$	18	7	4	67	4
$1t_2$	9	10	5	74	3
1e	0	13	6	80	1
$2t_2$	32	9	7	4	48
$2a_1$	0	16	6	13	65
$1t_1$	0	30	4	0	66
$3t_2$	0	7	7	5	80
$4t_2$	3	15	4	0	76
2e	0	0	4	2	94
$2t_1$	0	0	4	0	96
$3a_1$	49	31	11	8	1
$4t_2$	18	48	6	2	26

Table VIII. Atomic Populations in Molecular Orbitals of P_4O_{10}

	atomic pop., %						
	P			–O–		O=	
orbital	3s	3p	3d	2s	2p	2s	2p
$1a_1$	23	6	1	61	6	3	1
$1t_2$	14	10	1	63	4	6	1
1e	0	19	2	78	2	0	0
$2t_2$	6	19	2	9	1	58	6
$2a_1$	4	21	1	4	1	64	6
$3t_2$	5	33	1	3	53	5	1
$1t_1$	0	32	2	0	61	0	5
$3a_1$	1	18	2	12	65	0	0
$4t_2$	0	13	2	0	84	0	0
$5t_2$	1	11	1	0	61	0	26
$4a_1$	7	2	0	2	0	20	69
2e	0	1	9	2	79	0	9
$2t_1$	0	4	1	0	95	0	0
$6t_2$	1	2	3	0	28	11	55
3e	0	5	13	3	12	0	66
$7t_2$	1	6	10	2	8	0	74
$3t_1$	0	13	3	0	9	0	75

basis. The latter figure contrasts with the much lower phosphorus 3d contribution to P–O–P bonds (s:p:d = 1:1.3:0.3). These figures confirm the view that the pentavalence in phosphorus (V) oxide is poorly described in terms of classical sp^3d hybridization: the apical oxygen–phosphorus linkage is instead best described in terms of p_σ donation and d_π ac-

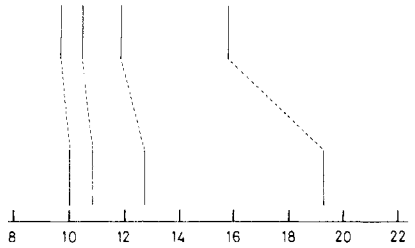

Figure 6. Correlation between experimental ionization energies for P_4 and those deduced by application of Koopmans' theorem to ab initio orbital energies (horizontal axis: ionization energy/eV).

ceptance by phosphorus, analogous to the bonding between PF_3 and transition metals.

PE Spectra of P_4, P_4O_6, and P_4O_{10}. PE spectra of phosphorus have been reported previously[12,13] and are not reproduced in the present work. However, Figure 6 shows the correlation between experimental ionization energies for the P_4 molecule and orbital energies derived from the ab initio calculation in the spd basis. It is clear that application of Koopmans' theorem to our theoretical results leads to the conventional assignment for the PE spectrum of the P_4 molecule.

The helium(I) PE spectrum of P_4O_6 contains five well-defined bands; an extra band is apparent at higher binding energy in the helium(II) spectrum. Our calculations yield groupings of orbital energies which clearly suggest the assignment adopted in Table I and displayed graphically in Figure 2. The pleasing correspondence between experimental ionization energies and those deduced by application of Koopmans' theorem to calculated eigenvalues indicates that differential relaxation effects and correlation energy changes are of minor importance for P_4O_6. The absolute values for orbital energies (ϵ_i) are not of course equal and opposite to observed ionization energies ($(IE)_i$), but a linear correlation between the two sets of data of the form $-(IE)_i = a\epsilon_i + b$ seems to hold. The values of a and b are of no importance to the present work.

The more complicated electronic structure of P_4O_{10} inevitably makes for a difficult assignment problem. However, there is a clear qualitative resemblance between He II spectra of P_4O_6 and P_4O_{10} in the high binding energy region (i.e., for the four bands at highest binding energy), and it is gratifying to find that our calculations suggest direct correlations between the electronic energy levels associated with these features. The calculations further suggest that the three leading PE bands should be associated with the t_1, t_2, and e apical oxygen p_π molecular orbitals. The remaining four molecular levels are assigned to the prominent PE band at 15.36 eV in the He I spectrum. Significant attenuation of this band is apparent under He II excitation.

On the basis of these assignments it is possible to construct a correlation diagram (Figure 7) relating empirical subshell ionization energies for the molecules P_4, P_4O_6, and P_4O_{10}. In constructing this diagram we are of course guided by the restriction that crossing of levels within a given symmetry manifold is forbidden.

In going from P_4 to P_4O_6 there is remarkably little change in the energy of the phosphorus lone pairs $t_2 + a_1$. This is somewhat surprising in view of the undoubted increase in partial positive charge on the phosphorus atom and presumably reflects mixing with more tightly bound symmetry orbitals derived from oxygen atoms. A similar effect must also account for the very marked destabilization of the phosphorus 3s combination of a_1 symmetry: as noted previously the level correlating with the totally symmetric P 3s subshell of P_4 has very little 3s character in P_4O_6. By contrast the 3s combination of t_2 symmetry shows little change in atomic character and the expected stabilization in going from P_4 to P_4O_6. The

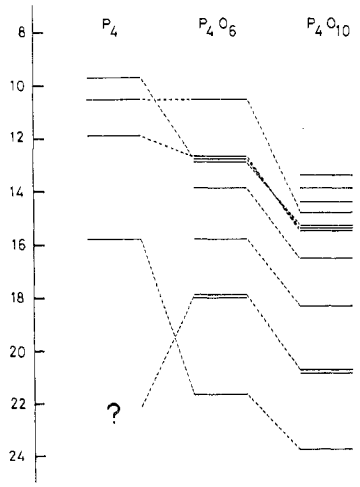

Figure 7. Correlation between experimental ionization energies for P_4, P_4O_6, and P_4O_{10} (vertical axis: ionization energy/eV).

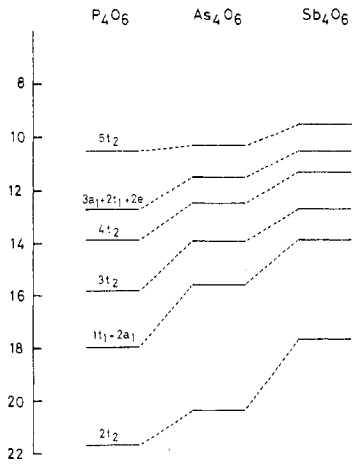

Figure 8. Correlation between experimental ionization energies for P_4O_6, As_4O_6, and Sb_4O_6 (vertical axis: ionization energy/eV).

remaining e level also shows a pronounced stabilization in going from P_4 to P_4O_6. New levels of P_4O_6 having no counterpart in the molecule P_4 are of symmetries $t_1 + t_2 + t_1 + t_2$.

The relationship between electronic energy levels in P_4O_6 and P_4O_{10} is rather more straightforward. As expected, the P lone-pair levels show a pronounced stabilization as a result of interaction with the apical oxygen acceptor atoms. The stabilization of the other levels can be understood in terms of the increasing partial positive charge on phosphorus and decreasing partial negative charge on bridging oxygen in going from P_4O_6 to P_4O_{10}.

PE Spectra of As_4O_6 and Sb_4O_6. The remarkable qualitative resemblance between PE spectra of P_4O_6, As_4O_6, and Sb_4O_6 suggests that the assignment proposed on the basis of the calculations on P_4O_6 carries over to heavier oxides in the series. It is therefore possible to construct the empirical correlation diagram shown in Figure 8 relating ionic levels for the group 5 oxides.

Several trends apparent from this figure deserve comment. First we note that all levels are progressively destabilized in the series P_4O_6—As_4O_6—Sb_4O_6. For levels of dominant oxygen 2p atomic character this must reflect increasing partial negative charge on the oxygen atoms as the electronegativity difference between oxygen and the relevant group 5 atom increases. For metal-based levels, in particular to t_2 lone-pair and metal s t_2 combinations, the observed variations in ionization energy appear to reflect variations in atomic ionization

energies. We note that a pronounced "alternation effect" is apparent in that the differences in ionization energies between P_4O_6 and As_4O_6 are much less pronounced than those between As_4O_6 and Sb_4O_6. Similar effects are found in PE spectra of the group 5 hydrides[23] and halides.[24,25]

We turn attention now to discussion of fine structure apparent in the first band in PE spectra of As_4O_6 and Sb_4O_6. In their study of the arsenic compound Cannington and Whitfield[26] assumed that the first band represented three distinct ionization processes involving arsenic and oxygen lone pairs, although they failed to venture an assignment in terms of symmetry labels appropriate to tetrahedral systems. However there is no marked change in the profile of this band on switching from He I to He II excitation, as would be expected if it were associated with molecular subshells having very different ionization cross-section profiles. We prefer the alternative view that the first band relates uniquely to the t_2 lone-pair combination. Consistent with this idea, there is a marked decrease in the intensity of the first band in the spectrum relative to the third band (the latter feature being associated with an O 2p lone-pair combination) on switching from He I to He II excitation.

The fine structure in the spectra could in principle arise from either spin–orbit coupling or vibronic (Jahn–Teller) distortion in the molecular ion or from both. The absence of fine structure in the spectrum of P_4O_6 certainly invites the speculation that spin–orbit coupling is of major importance in mediating appearance of the fine structure. However, spin–orbit coupling can assume significant proportions only if there is substantial mixing between the t_2 lone-pair combination and a t_2 combination containing a significant contribution from As p orbitals directed perpendicular to the lone pairs. Our calculations indicate that mixing of this sort is not of major importance and we therefore come to the alternative view that the structure is due largely to Jahn–Teller distortion. Vibronic structure of this sort is quite common in PE spectra of high-symmetry cage systems including P_4,[12,13] adamantane,[27–29] and bullvalene.[30]

Concluding Remarks. Our combined experimental and theoretical investigation confirms the conventional description of the bonding in the group 5 oxides. In particular it appears that cross-cage interactions are of minor importance for the molecules studied in the present work. This contrasts with the situation found in N_4S_4[31] where cross-cage bonding is significant. Investigations of the electronic structure of other group 5 chalcogenides are already at hand, a particular aim of the work being to explore the limitations of "classical" descriptions of bonding in cage molecules. These matters will be the subject of future publications.

Acknowledgment. The equipment used in this work was financed by the Science Research Council (U.K.). R.G.E. wishes to thank Wolfson College, Oxford, for the award of a Junior Research Fellowship.

Registry No. P_4O_6, 10248-58-5; As_4O_6, 36533-93-4; Sb_4O_6, 72926-13-7; P_4O_{10}, 16752-60-6; P_4, 12185-10-3.

(23) Potts, A. W.; Price, W. C. *Proc. R. Soc. London, Ser. A* **1972**, *326*, 181.
(24) Potts, A. W.; Lempka, H. J.; Streets, D. G.; Price, W. C. *Philos. Trans. R. Soc. London, Ser. A* **1970**, *268*, 59.
(25) Nicholson, D. G.; Rademacher, P. *Acta Chem. Scand., Ser. A* **1974**, *28*, 1136.
(26) Cannington, P. M.; Whitfield, H. J. *J. Electron Spectrosc. Relat. Phenom.* **1977**, *10*, 35.
(27) Worley, S. D. *J. Electron Spectrosc. Relat. Phenom.* **1975**, *6*, 157.
(28) Boschi, R.; Schmidt, W.; Suffolk, R. J.; Wilkins, B. T.; Lempka, H. J.; Ridyard, J. N. A. *J. Electron Spectrosc. Relat. Phenom.* **1973**, *2*, 377.
(29) Schmidt, W. *J. Electron Spectrosc. Relat. Phenom.* **1975**, *6*, 163.
(30) Bischof, P.; Gleiter, R.; Heilbronner, E.; Hornung, V.; Schroder, G. *Helv. Chim. Acta* **1970**, *53*, 1645.
(31) Findlay, R. H.; Palmer, M. H.; Downs, A. J.; Egdell, R. G.; Evans, R., companion paper in this issue.

Contribution from the Department of Analytical Chemistry and Radiochemistry, University of Liège, Sart Tilman, Liège, B-4000 Belgium

Nuclear Magnetic Resonance Spectroscopy of Lanthanide Complexes with a Tetraacetic Tetraaza Macrocycle. Unusual Conformation Properties[1]

J. F. DESREUX

Received August 8, 1979

The ^1H and ^{13}C NMR spectra of diamagnetic and paramagnetic lanthanide complexes with 1,4,7,10-tetraazacyclododecane-*N*,*N'*,*N''*,*N'''*-tetraacetic acid (DOTA) are analyzed in terms of the stereodynamic behavior of the macrocycle and of the lability of the acetate groups. Below room temperature, the ethylenic groups are rigid on the NMR time scale. Rapid ring inversion is achieved at elevated temperature, the energy barrier being very high. The following kinetic parameters are obtained by line-shape analysis in the case of LaDOTA: $\Delta G^*_{300} = 60.7 \pm 1.2$ kJ mol^{-1}, $\Delta H^* = 59.4 \pm 0.8$ kJ mol^{-1}, and $\Delta S^* = -4.6 \pm 3.3$ J K^{-1} mol^{-1}. Similar energy barriers are measured for paramagnetic complexes. All the ethylenic groups of the macrocycle adopt the same conformation at low temperatures. This spatial arrangement leads to a new type of temperature-dependent asymmetry which appears in the NMR spectra of the labile acetate groups. The structure of the Eu(III), Pr(III), and Yb(III) complexes with DOTA is deduced from the relative magnitude of the large paramagnetic shifts exhibited by these compounds. The nitrogen–lanthanide distance is approximately 2.85 Å, and the metal is located under the macrocycle.

Introduction

Current interest in the complexing properties of macrocycles[2] has stimulated the synthesis and study of a large number of new cyclic polyoxa and polyaza ligands. A variety of macrocycles of different cavity size and rigidity is now available to the coordination chemist, but most of these compounds still suffer from the absence of ionizable functions, a deficiency which is not presented by more classical ligands. However, a macrocycle featuring ionizable functions should combine two decided advantages: a selectivity gained from the steric requirements of the internal cavity and a pH-sensitive complexation. So far, only a few members of this new class of cyclic ligands are known. Recent reports describe the preparation and properties of macrocycles containing one or

(1) Portions of this work were presented at the 34th Annual Southwest Regional Meeting of the American Chemical Society, Corpus Christi, Texas, Nov 1978.
(2) J. J. Christensen, D. J. Eatough, and R. M. Izatt, *Chem. Rev.*, **74**, 351 (1974).

0020-1669/80/1319-1319$01.00/0